Two-Dimensional Warping for One-Dimensional Signals—Conceptual Framework and Application to ECG Processing

Martin Schmidt, Mathias Baumert, *Senior Member, IEEE*, Alberto Porta, *Member, IEEE*, Hagen Malberg, and Sebastian Zaunseder

***Abstract*—We propose a novel method for evaluating the similarity between two 1d patterns. Our method, referred to as two-dimensional signal warping (2DSW), extends the basic ideas of known warping techniques such as dynamic time warping and correlation optimized warping. By employing two-dimensional piecewise stretching 2DSW is able to take into account inhomogeneous variations of shapes. We apply 2DSW to ECG recordings to extract beat-to-beat variability in QT intervals (QTV) that is indicative of ventricular repolarization lability and typically characterised by a low signal-to-noise ratio. Simulation studies show high robustness of our approach in presence of typical ECG artefacts. Comparison of short-term ECG recorded in normal subjects versus patients with myocardial infarction (MI) shows significantly increased QTV in patients (normal subject 2.36 ms $\pm$ 1.05 ms vs. MI patients 5.94 ms $\pm$ 5.23 ms (mean $\pm$ std), $p < 0.001$). Evaluation of a standard QT database shows that 2DSW allows highly accurate tracking of QRS-onset and T-end. In conclusion, the two-dimensional warping approach introduced here is able to detect subtle changes in noisy quasi-periodic biomedical signals such as ECG and may have diagnostic potential for measuring repolarization lability in MI patients. In more general terms, the proposed method provides a novel means for morphological characterization of 1d signals.**

***Index Terms*—Dynamic time warping, ECG, QT, QT interval, QT variability, signal processing, two-dimensional warping, warping.**

I. Introduction

In signal and image processing *warping* is understood as a technique to match two patterns. By allowing certain variations to one pattern's shape, warping accounts for temporal shifts to occur within patterns. A set of predefined rules determines which variations are allowed. A cost function guides the search for the optimal variation, i.e. the one that results in closely matched patterns.

Warping originated from the field of audio processing, where the influence of varying lengths in the pronunciation of identical phoneme need to be accounted for. Dynamic Time Warping (DTW), which is the most famous warping algorithm, was first introduced by Vintsyuk in 1968 [1]. DTW performs a sample-to-sample projection of one pattern to a reference pattern that aims at minimizing the Euclidean distance between the patterns. Velichko [2] and Sakoe and Chiba [3] applied and further enhanced DTW. Although DTW has been largely replaced by Hidden Markov Models in the field of audio processing, warping is used in various other fields today, including biometry [4], gene expression [5], pattern recognition [6] and biomedical signal processing [7], [8].

The widespread applicability of warping has produced various modifications and enhancements such as *Scaling Up-DTW* [9], *derivative* [10], *FastDTW* [11] and *Online Time Warping* [12]. Of the more substantial modifications to DTW that have been proposed, Correlation Optimized Warping (COW) [13] is probably the best known algorithm. Even COW can be considered a representative of DTW under certain circumstances [14]. The close relationship becomes evident when thinking of aforementioned DTW variants that make use of subsampling and/or interpolation schemes, which implicitly pursue ideas similar to COW. However, a conceptual difference between COW and DTW can be seen in their strategies of comparing and aligning patterns: whereas DTW originally aligns patterns on a sample-to-sample basis, COW makes use of segmentation. Using segments allows COW to rely on correlation as measure of similarity between segments. In comparative studies, in particular related to chromatography, COW was proven to be beneficial when compared to DTW [14]–[16]. Despite the methodological differences and diverse application areas, all aforementioned methods are unified by their goal to account for 1d shifts (shift in time or, in case of chromatography, in frequency).

Physiological processes are most often the result of highly complex interactions. As a consequence quasi-periodic events such as deflections in the body surface electrocardiogram (ECG), which are related to the cardiac cycle are expected to change in height, width and morphology [7] in a much more complex way than it is addressed by current warping techniques. To measure the similarity of such physiological patterns it might be necessary to allow for more complex adaptation.

Manuscript received March 11, 2014; revised July 09, 2014 and August 26, 2014; accepted August 26, 2014. Date of publication September 04, 2014; date of current version October 03, 2014. The associate editor coordinating the review of this manuscript and approving it for publication was Dr. Chong-Yung Chi. This work was supported by the German Academic Exchange Service (DAAD) and the Group of Eight Australia.

M. Schmidt, H. Malberg, and S. Zaunseder are with the Institute of Biomedical Engineering, TU Dresden, Dresden, Saxony 01069, Germany (e-mail: martin_schmidt@tu-dresden.de; hagen.malberg@tu-dresden.de; sebastian.zaunseder@tu-dresden.de).

M. Baumert is with the School of Electronics and Electrical Engineering, University of Adelaide, Adelaide, South Australia SA 5005, Australia (e-mail: mathias.baumert@adelaide.edu.au).

A. Porta is with Department of Biomedical Sciences for Health, Galeazzi Orthopedic Institute, University of Milan, Milan 20122, Italy (e-mail: alberto.porta@unimi.it).

Digital Object Identifier 10.1109/TSP.2014.2354313

Similarity and matching have been quantified to measure subtle changes in time intervals from ECG, particularly the QT interval. Increased beat-to-beat variability of QT intervals (QTV) was shown to be a strong predictor of cardiac mortality [17]. Recent works applied modern signal processing strategies to deepen the understanding of QT variability [18]–[22] and its extraction in face of noise and artifacts. ECG artifacts that are typically encountered in long-term recordings remain a challenge. The QT interval comprises the time interval of ventricular de- and repolarization, i.e. QRS complex and ST-T segment in ECG. While the duration of the QRS complex can be considered rather stable, the ST-T segment duration changes notably, depending on heart rate and autonomic tone. A widely used algorithm to determine beat-to-beat QT interval variability relies on homogeneously stretching the ST-T segment of the beat under consideration until it matches best a ST-T template [23]. Based on pre-defined borders of Q peak and ST-T segment in the template, the QT interval of the beat under consideration can be calculated by considering the optimal stretch. The algorithm provides reliable results and was successfully used in many clinical studies [17], [24]. From a physiological point of view such homogeneous stretching might not be able to capture details of morphological changes within the QT interval. To account for more complex modifications, Vullings *et al.* [8] and Zifan *et al.* [25] extracted ECG time intervals in a more flexible manner by allowing inhomogeneous stretching, using DTW and a modified version of derivative DTW, respectively.

Since existing warping techniques do not cover the wide spectrum of physiologically plausible variations the aim of our work was to develop a technique that complies with the physiological reality by allowing for temporal shifts and changes in magnitude at the same time. We propose two-dimensional signal warping (2DSW) as a powerful tool that enables complex adaptations. We apply this technique to measure QT variability to exemplify its potential.

The remainder of the article is structured as follows: in Section II we introduce the concept of 2DSW, provide the theoretical framework and present an implementation of its basic functionality. Section III covers the integration of 2DSW into a scheme to estimate QT interval variability in surface ECG. Section IV contains the results of computational considerations as well as the application to simulated and real ECG. Sections V and VI discuss our results and highlight future developments and applications.

II. Two-Dimensional Warping of One-Dimensional Signals

A. Basic Notation

Two-dimensional warping adapts a waveform to a reference waveform by accounting for differences in time and amplitude. Therefore, a *warping grid* is superimposed on the waveform to be adapted (see Fig. 1). The warping grid establishes N_c column and N_r row borders. The intersection points of the warping grid define so-called *warping points* denoted as P. Each P_i with $i \in \{1, 2, \ldots, N_P\}$ and $N_P = N_c \cdot N_r$ is defined by its absolute position $\boldsymbol{p}_i = [x_i, y_i]$ in a two dimensional space and its position

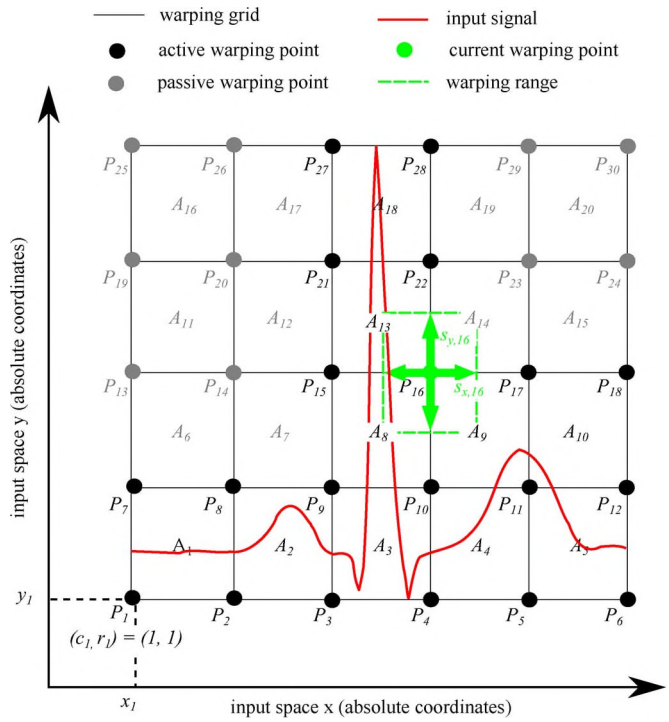

Fig. 1. Notation of 2DSW's basic elements for an exemplary grid of size $N_c = 6$ and $N_r = 5$ and rectangular warping areas.

in the warping grid $\boldsymbol{q}_i = [c_i, r_i]$, where c_i specifies the column and r_i the row of P_i. Note that index i is incremented over columns first. $\mathcal{P}$ defines the set of all ordered pairs $(\boldsymbol{q}_i, \boldsymbol{p}_i)$ with $|\mathcal{P}| = N_P$ to

$$\mathcal{P} = \{(\boldsymbol{q}_i, \boldsymbol{p}_i) | \boldsymbol{q}_i \in \{1, 2, \ldots, N_c\} \times \{1, 2, \ldots, N_r\}, \boldsymbol{p}_i \in \mathbb{R}^2 \; \forall i \in \{1, 2, \ldots, N_P\}\}. \quad (1)$$

In the remainder P_i is used as identifier of a warping point when its absolute coordinates or its grid position are not addressed specifically.

Given a quadrangle spanned by four warping points P_i, P_{i+1}, P_{i+N_c+1} and P_{i+N_c} with $c_i < N_c$ and $r_i < N_r$, its lower boundary $\boldsymbol{a}$, i.e. the line connecting P_i and P_{i+1}, can be expressed as

$$\begin{aligned} \boldsymbol{a} &= [a_x(\lambda_a), a_y(\lambda_a)] \\ &= (\boldsymbol{p}_{i+1} - \boldsymbol{p}_i) \cdot \lambda_a + \boldsymbol{p}_i \qquad \lambda_a \in [0, 1] \end{aligned} \quad (2)$$

with its components

$$a_x(\lambda_a) = (x_{i+1} - x_i) \cdot \lambda_a + x_i \quad \lambda_a \in [0, 1] \quad (3)$$

$$a_y(\lambda_a) = (y_{i+1} - y_i) \cdot \lambda_a + y_i, \quad \lambda_a \in [0, 1] \quad (4)$$

where λ_a is a scalar. The length of line $\boldsymbol{a}$, i.e. between P_i and P_{i+1}, in x-direction and y-direction, respectively, is thus given by

$$|x_{i+1} - x_i| \rightarrow \mathrm{x-length\ of}\ \boldsymbol{a} \quad (5)$$

$$|y_{i+1} - y_i| \rightarrow \mathrm{y-length\ of}\ \boldsymbol{a} \quad (6)$$

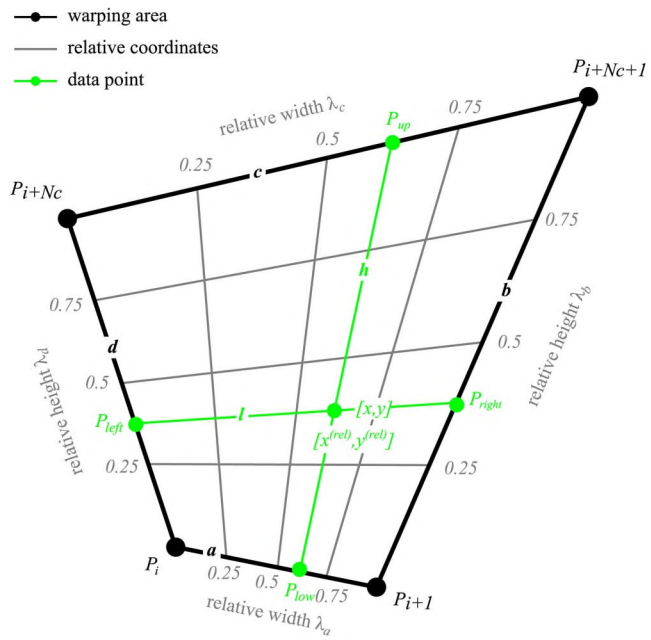

Fig. 2. Illustration of the position of an arbitrary point in a non-rectangular warping area.

In analogy to (2) we define lines $\boldsymbol{b}$, $\boldsymbol{c}$ and $\boldsymbol{d}$, where $\boldsymbol{b}$ connects $P_i + 1$ and P_{i+1+N_c} with $c_i < N_c$ and $r_i < N_r$ and so forth (see Fig. 2) such that

$$\begin{aligned}\boldsymbol{b} &= [b_x(\lambda_b), b_y(\lambda_b)] \\ &= (\boldsymbol{p}_{i+N_c+1} - \boldsymbol{p}_{i+1}) \cdot \lambda_b + \boldsymbol{p}_{i+1} \quad \lambda_b \in [0,1] \qquad (7)\\ \boldsymbol{c} &= [c_x(\lambda_c), c_y(\lambda_c)] \\ &= \left(\boldsymbol{p}_{i+N_c+1} - \boldsymbol{p}_{i+N_c}\right) \cdot \lambda_c + \boldsymbol{p}_{i+N_c} \quad \lambda_c \in [0,1] \qquad (8)\\ \boldsymbol{d} &= [d_x(\lambda_d), d_y(\lambda_d)] \\ &= \left(\boldsymbol{p}_{i+N_c} - \boldsymbol{p}_i\right) \cdot \lambda_d + \boldsymbol{p}_i \quad \lambda_d \in [0,1] \qquad (9)\end{aligned}$$

Let A be the area of the quadrangle spanned by four warping points. Using the aforementioned definitions A can be described as the set of points $[x, y]$ for which holds

$$\begin{aligned}A = \Bigg\{ [x,y] \in \mathbb{R}^2 | y \geq a_y \left(\frac{|x - x_i|}{|x_{i+1} - x_i|} \right) \quad \wedge \\ y \leq c_y \left(\frac{|x - x_{i+N_c}|}{|x_{i+N_c+1} - x_i + N_c|} \right) \quad \wedge \\ x \geq d_x \left(\frac{|y - y_i|}{|y_{i+N_c} - y_i|} \right) \quad \wedge \\ x \leq b_x \left(\frac{|y - y_{i+1}|}{|y_{i+N_c+1} - y_{i+1}|} \right) \Bigg\} \qquad (10)\end{aligned}$$

where the right-hand side bracketed terms, which use the definitions from (2)to (7), account for the fact that A is not necessarily rectangular nor paraxial to the abscissa or ordinate. An area A defined by four neighboring warping points is referred to as *warping area*. A grid as previously introduced imposes N_A areas A_j with $j = 1, 2, \ldots, N_A$, where $N_A = (N_c - 1) \cdot (N_r - 1)$. Indexing A_j starts in the left lower corner of the grid and increments through the column first.

A warping point is said to be an *active warping point* $P_i^{(1)}$ if it contains a part of the waveform in at least one of his four adjacent areas. Points that do not fulfill this condition are referred to as *passive warping points* $P_i^{(0)}$. The sets of active and passive warping points form again the set $\mathcal{P}$, i.e. $\mathcal{P}^{(1)} \cap \mathcal{P}^{(0)} = \emptyset$ and $\mathcal{P}^{(1)} \cup \mathcal{P}^{(0)} = \mathcal{P}$.

B. Warping Concept

2DSW is accomplished by primarily shifting active warping points. A shift of a point P_i by $\boldsymbol{s}_i$ affects $\boldsymbol{p}_i$, i.e.

$$P_i' := (\boldsymbol{p}_i + \boldsymbol{s}_i, \boldsymbol{q}_i) = (\boldsymbol{p}_i', \boldsymbol{q}_i)\,. \qquad (11)$$

Any shift of one or more warping points adjacent to a warping area A_j results in a modified warping area denoted as A_j' that is defined by its adapted boundaries $\boldsymbol{a}', \boldsymbol{b}', \boldsymbol{c}'$ and $\boldsymbol{d}'$. Waveform segments within A_j are consecutively adapted according to the change in the area they belong to.

The rules for deforming a waveform in the 2DSW process are based on absolute coordinates, i.e. those belonging to the input space, and relative coordinates, i.e. those which are defined in relation to a warping area's boundaries. Shortly, given a point $[x, y] \in A_j$, where A_j is an arbitrary warping area, 2DSW shifts this point in such a way that its coordinates $[x^{(rel)}, y^{(rel)}]$ relative with respect to A_j' remain unchanged, i.e. $[x^{(rel)}, y^{(rel)}] = [x'^{(rel)}, y'^{(rel)}]$. Fig. 2 and Fig. 3 illustrate the process (the underlying mathematical consideration is given below).

Searching for the $\boldsymbol{s}_i$ that allows for the optimal waveform deformation is guided by minimizing a cost function, which maximizes the similarity between the waveform to be adapted and its reference.

C. Mathematical Framework of Waveform Deformation

After having outlined the concept, the following section details the mathematical framework which underlies the deformation of a waveform during 2DSW.

Let $\boldsymbol{a}$ and $\boldsymbol{c}$ be the lower and upper boundaries of A. Given any point $[x, y] \in A$ its relative abscissa $x^{(rel)}$ is determined by finding the points $P_{up} \in \boldsymbol{c}$ and $P_{low} \in \boldsymbol{a}$ for which

$$\begin{aligned}\frac{|x_{up} - x_{i+N_c}|}{|x_{i+N_c+1} - x_{i+N_c}|} &\stackrel{!}{=} \frac{|x_{low} - x_i|}{|x_{i+1} - x_i|} \\ [x,y] &\stackrel{!}{\in} \boldsymbol{h}, \qquad (12)\end{aligned}$$

where $\boldsymbol{h} = (\boldsymbol{p}_{up} - \boldsymbol{p}_{low}) \cdot \lambda_h + \boldsymbol{p}_{low}$ for $\lambda_h \in [0, 1]$.

Here $\boldsymbol{h}$ denotes the line connecting P_{low} and P_{up}. Following the identification of P_{low} and P_{up} the relative abscissa $x^{(rel)}$ is calculated as

$$x^{(rel)} = \frac{|x_{up} - x_{i+N_c}|}{|x_{i+N_c+1} - x_{i+N_c}|} = \frac{|x_{low} - x_i|}{|x_{i+1} - x_i|}. \qquad (13)$$

Similarly, the relative ordinate $y^{(rel)}$ is determined by finding $P_{right} \in \boldsymbol{b}$ and $P_{left} \in \boldsymbol{d}$ for which holds

$$\begin{aligned}\frac{|y_{left} - y_i|}{|y_{i+N_c} - y_i|} &\stackrel{!}{=} \frac{|y_{right} - y_{i+1}|}{|y_{i+N_c+1} - y_{i+1}|} \\ [x,y] &\stackrel{!}{\in} \boldsymbol{l}, \qquad (14)\end{aligned}$$

where $\boldsymbol{l} = (\boldsymbol{p}_{right} - \boldsymbol{p}_{left}) \cdot \lambda_l + \boldsymbol{p}_{left}$ for $\lambda_l \in [0, 1]$.

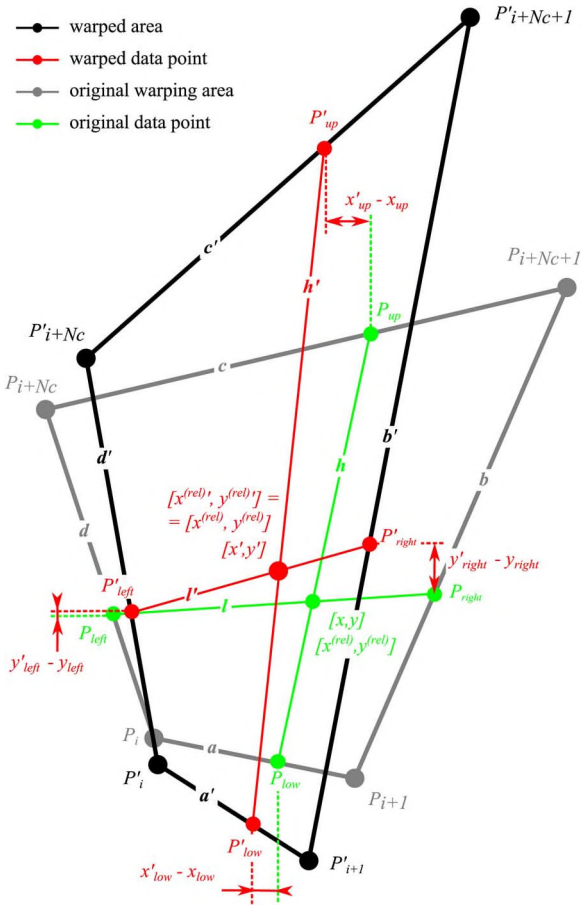

Fig. 3. Illustration of the effect of 2DSW on the area and point exemplified in Fig. 2.

Here $\boldsymbol{l}$ is the line connecting P_{left} and P_{right}. The relative ordinate $y^{(rel)}$ is computed as

$$y^{(rel)} = \frac{|y_{left} - y_i|}{|y_{i+N_c} - y_i|} = \frac{|y_{right} - y_{i+1}|}{|y_{i+N_c+1} - y_{i+1}|}. \tag{15}$$

Fig. 2 gives a graphical example of the initial situation.

Now consider any shift by $\boldsymbol{s}_k$ so that $P_k \rightarrow P'_k$ with $k \subset \{i, i+1, i+N_c, i+N_c+1\}$, changing A to A' and its boundaries to $\boldsymbol{a}'$, $\boldsymbol{b}'$, $\boldsymbol{c}'$ and $\boldsymbol{d}'$, respectively (see Fig. 3). For a single point $[x, y] \in A$ warping aims at finding $[x', y']$, which maintains its relative coordinates with respect to A'. Thus, its new abscissa is given by

$$\begin{aligned} x' &= x + \Delta x \cdot y^{(rel)} \\ \text{with} \quad \Delta x &= \left(x'_{up} - x_{up}\right) - \left(x'_{low} - x_{low}\right), \\ \text{with} \quad \boldsymbol{p}'_{up} &= \left[x'_{up}, y'_{up}\right] = \left[c'_x\left(x^{(rel)}\right), c'_y\left(x^{(rel)}\right)\right], \\ \text{and} \quad \boldsymbol{p}'_{low} &= \left[x'_{low}, y'_{low}\right] = \left[a'_x\left(x^{(rel)}\right), a'_y\left(x^{(rel)}\right)\right]. \end{aligned} \tag{16}$$

In (16) the expression Δx is the absolute displacement in x-direction defined by the displacement of points P_{up} and P_{low}. The factor $x^{(rel)}$ considers this absolute displacement proportionately and adds the portion to the original position x.

In analogy for the ordinate it holds

$$\begin{aligned} y' &= y + \Delta y \cdot x^{(rel)} \\ \text{with} \quad \Delta y &= \left(y'_{right} - y_{right}\right) - \left(y'_{left} - y_{left}\right) \\ \text{with} \quad \boldsymbol{p}'_{left} &= \left[x'_{left}, y'_{left}\right] = \left[d'_x\left(y^{(rel)}\right), d'_y\left(y^{(rel)}\right)\right] \\ \text{and} \quad \boldsymbol{p}'_{right} &= \left[x'_{right}, y'_{right}\right] = \left[b'_x\left(y^{(rel)}\right), b'_y\left(y^{(rel)}\right)\right]. \end{aligned} \tag{17}$$

Fig. 3 gives an example for 2DSW of a single point and illustrates the elements of (16) and (17).

When dealing with a function or waveform instead of a single point, the waveform can be considered as a set $\mathcal{Y}$ of vectors $[x, y]$, $\mathcal{Y} = \{[x, y] | \in \mathbb{R} \times \mathbb{R}\}$. If the set $\mathcal{Y}$ represents a waveform, then between single pairs $[x_i, y_i]$ and $[x_j, y_j]$ it must hold $x_i \neq x_j \; \forall i \neq j$. Unequal x values result from the functional relationship of the waveform, i.e. for each x value there is only one y value. X and Y denote the series of x and y values, i.e. x_i and y_i for $i \in \{1, 2, \ldots, |\mathcal{Y}|\}$, contained in $\mathcal{Y}$ and sorted in ascending order of the x-value of each pair. The waveform belonging to area A_j, denoted as $\mathcal{Y}_j$, is given by $\mathcal{Y}_j = \{[x, y] | [x, y] \in A_j\}$. By defining a waveform as a set of vectors the previously given ideas on shifting a single point are extended to waveforms.

D. Waveform Comparison and Cost Function

The shifting of P_i and its resulting deformation aims at minimizing the cost function between the waveform to be adapted and the reference waveform. As cost function we use the normalized Euclidean distance, which has previously been applied to similar problems [1], [26]. The normalized Euclidean distance $d^{(2n)}(.)$ between the sets of vectors $\mathcal{Y}^{(1)}$ and $\mathcal{Y}^{(2)}$ with $X^{(1)} \stackrel{!}{=} X^{(2)}$ is given by

$$d^{(2n)}\left(Y^{(1)}, Y^{(2)}\right) = \frac{\sqrt{\sum_{i=1}^{|\mathcal{Y}|}\left(y_i^{(1)} - y_i^{(2)}\right)^2}}{|\mathcal{Y}|}, \tag{18}$$

where $Y^{(1)}$ and $Y^{(2)}$ denote the y values of the vectors $\mathcal{Y}^{(1)}$ and $\mathcal{Y}^{(2)}$. Compared to the Euclidean distance its normalized version accounts for the range in which two sets are compared. The condition $X^{(1)} \stackrel{!}{=} X^{(2)}$ ensures identical domains of $X^{(.)}$. If the waveform to be adapted and the reference waveform do not fulfill this requirement an initial projection of their domains must be carried out. In practice, this might be the case for two waveforms sampled at different sampling rates of which one must be linearly scaled (i.e. interpolated/down sampled).

E. Shifting Constraints Of Warping Points

To allow for a flexible adaptation only few constraints should be imposed to the shifting of warping points. One constraint is to preserve the functional character of the waveform to be adapted, i.e. warping points are not allowed to change in a way that the adapted waveform has multiple y-values for a single x value. A second constraint, which similarly exists in other warping techniques, imposes a maximum range to each warping point in which it is allowed to move (see the *warping range* in Fig. 1). The warping range is specific to each warping point and defined

by the maximum deflection in both horizontal and vertical directions of P_i. The vector $\boldsymbol{s}_i^{(max)}$ denotes the resulting stretch of the warping range associated with P_i in x and y directions. The range restriction hinders warping areas to reduce below a given size, which may otherwise cause the cost function to produce misleading results. From a practical point of view this constraint also proves beneficial regarding the computational effort.

F. Algorithmic Implementation

Most of the concepts can be readily implemented. Considering the theoretical framework only the resolution $res^{(x)}$ and $res^{(y)}$ at which warping points are shifted needs to be defined. Practical choices of $res^{(x)}$ and $res^{(y)}$ are application dependent and specified in Section III-C.

To deal with the optimization problem we propose a heuristic procedure, which relies on three fundamentals: (1) sequential execution, (2) passive shifting and (3) local cost functions. Warping points are sequentially shifted. The order of shifting is chosen according to the index of the warping points. When point P_i is shifted by $\boldsymbol{s}_i$ those points P_j with $c_j \geq c_i \wedge r_j \geq r_i$ are equally shifted (referred to as passive shifting). As passive shifts apply only to j with $c_j \geq c_i \wedge r_j \geq r_i$, points, which have previously been actively shifted do not change their location afterwards. Note that passive shifting by identical $\boldsymbol{s}_i$ can cause the parallel translation of all points that define a warping area. In that case the waveform included in the area is not deformed but only displaced by $\boldsymbol{s}_i$. When searching for the $\boldsymbol{s}_i$ that optimizes the position $\boldsymbol{p}_i'$ of P_i in terms of a minimized cost function we restrict the range in which the cost function is calculated to those points that lie in adjacent warping areas of P_i (local cost function). The search for the optimal position is done in either one of two ways:

1) *Brute force*: Before shifting, the cost function is evaluated for all possible shifts inside the warping range. The results form the *adaptation matrix* $\boldsymbol{M}_i(\boldsymbol{s}) =: \boldsymbol{M}_i$ with $\boldsymbol{M}_i \in \mathbb{R}^{N_x \times N_y}$ with

$$N_{i,x} = \frac{s_x^{(max)}}{res^{(x)}} \quad \text{and} \quad N_{i,y} = \frac{s_y^{(max)}}{res^{(y)}}.$$

   In accordance with the pointwise definition of warping ranges, $N_{i,x}$ and $N_{i,y}$ are allowed to differ between P_i, leading to varying sizes of $\boldsymbol{M}_i$. The shift that results in the minimum of $\boldsymbol{M}_i$ is regarded as optimal shift.
2) *Fast search*: The fast search avoids computing all elements of $\boldsymbol{M}_i$, but sparsely calculates $\boldsymbol{M}_i$ by iteratively zooming into $\boldsymbol{M}_i$. Zooming refers to the creation of submatrices $\boldsymbol{M}_i^{\downarrow} \subset \boldsymbol{M}_i$ and $\boldsymbol{M}_i^{\downarrow\downarrow} \subset \boldsymbol{M}_i^{\downarrow}$ and so forth on different scales. A submatrix is extracted after evaluating the cost function of its predecessor matrix on a 5×5 grid. The grid spans the warping range associated with the preceeding matrix in a preferably uniform manner. Based on the calculated cost at the grid points those three with the minimum cost are searched that together span a new rectangular matrix $\boldsymbol{M}_i^{\downarrow}$. This procedure is repeated until the matrix size does not allow a grid of the defined size to be established. The costs of the last submatrix can be mapped to $\boldsymbol{M}_i(\boldsymbol{s})$, which now constitutes a sparse matrix. The minimum of this matrix defines the optimal shift.

Algorithm 1: Heuristic solution to 2DSW

Input: Pattern $\mathcal{Y}^{(1)}$, reference $\mathcal{Y}^{(2)}$
Define grid points $\mathcal{P}$;
Assign waveform to areas $\rightarrow \mathcal{Y}_j^{(1)}$;
for $i = 1, 2, \ldots, N_P$ **do**
  if $P_i \in \mathcal{P}^{(1)}$ **then**
    Calculate adaptation matrix $\boldsymbol{M}_i(\boldsymbol{s}_i)$;
    Get shift $\boldsymbol{s}_i = \underset{\boldsymbol{s}_i}{\operatorname{argmin}} \{\boldsymbol{M}_i(\boldsymbol{s}_i)\}$;
    for $j = i, 2, \ldots, P_N$ with $c_j \geq c_i \wedge r_j \geq r_i$ **do**
      Do shifting by $\boldsymbol{s}_i$ $(P_j \rightarrow P_j')$;
    end
  end
end
Output: $\mathcal{Y}^{(1)\prime}$

Algorithm 1 depicts pseudo code of the heuristic implementation of 2DSW. It should be noted that the heuristic procedure does not guarantee optimum matching, but empirical analyses suggests the method to produces satisfactory results in adequate computational time.

III. Application to QT Variability Assessment

A. General Description of the Warping Based Method

Fig. 4 contains the general framework for the analysis of QT variability using 2DSW. Structurally, our implementation resembles the classical template stretching approach [24]: define a template beat, allocate the QT interval in this template, adapt the template by 2DSW to each single beat and derive from each adapted version of the template the QT interval. The following sections details our implementation, including the parametrization of 2d warping. Pre- and postprocessing steps follow conventional ECG signal processing conventions and can be easily modified. However, the procedure should be regarded as an implementation whose components might be replaced by alternative algorithms or even semi-automated processing steps.

B. Preprocessing

QRS detection: If QRS annotations are available (applies for the used real data where the detections from [27] were used for the sake of comparison) they are readily used. If not, the algorithm by Afonso *et al.* [28] included in the biosig toolbox [29] is applied.

Signal filtering: Digital high pass filter (cut-off frequency 0.3 Hz) is applied to the raw ECG (for real data only).

QT extraction: Time delay estimation (TDE) by the Improved Woody's Method [30] is used initially to temporally adjust annotations. The Improved Woody's Method displaces annotations in the way that the correlation of annotations' surrounding signal segments is maximized. TDE is applied to signal segments of 100 ms, which are initially centered around the detections (100 ms are used as the approximated maximum QRS width). By optimizing the joint similarity TDE yields temporal aligned beat locations $t_{QRS,i}$. For each beat i a predefined QT window represented by the samples between $t_{Ton,i}$ and $t_{end,i}$

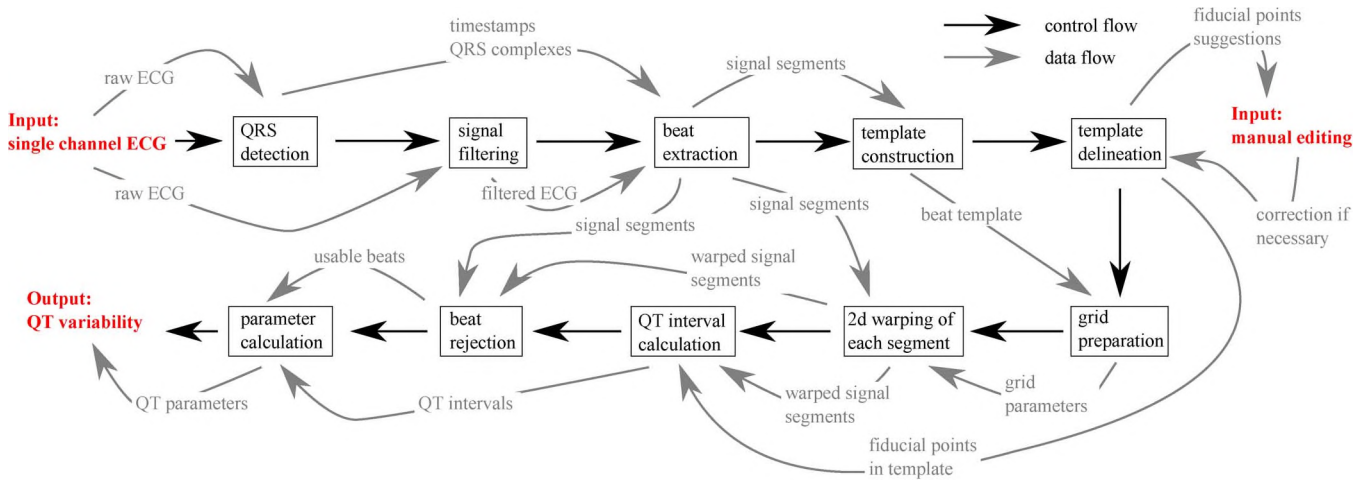

Fig. 4. General scheme of QT variability using 2DSW. Boxed items indicate processing steps.

is than extracted. Based on Laguna *et al.* [31] $t_{Ton,i}$ and $t_{Tend,i}$ are calculated as

$$t_{Ton,i} = t_{QRS,i} - 170\ \text{ms}$$
$$t_{Tend,i} = \begin{cases} t_{QRS,i+1} - 240\ \text{ms}, & \overline{RR} \geq 720\ \text{ms} \\ t_{QRS,i} + \frac{2}{3}\overline{RR}, & \overline{RR} < 720\ \text{ms}, \end{cases} \quad (19)$$

where $\overline{RR}$ represents the mean RR-interval over all beats. Equation (19) was chosen because it typically yields a segment that exceeds the actual QT window.

Template construction: To construct the waveform template all detected beats occurring in the first 100 s of a record are considered. The 100 s window was set empirically. What one would expect by using shorter time periods is a reduced suppression of noise by coherent averaging [32]. Those QT windows are excluded, whose normalized Manhattan distance, given by

$$d^{(2n)}\left(Y^{(1)}, Y^{(2)}\right) = \frac{\sum_{i=1}^{|\mathcal{Y}|} \left| y_i^{(1)} - y_i^{(2)} \right|}{|\mathcal{Y}|}, \quad (20)$$

to the mean QT window exceeds a empirically predefined threshold of 30 $\mu\text{V/ms}$. If less than 50% of the QT windows remain, all beats in a window shifted by 50 s are used for template construction. The predefined threshold is increased by 20 $\mu\text{V/ms}$ when the end of the signal has been reached and no window with more than 50% remaining QT windows has been found. The average of the remaining QT windows is used as template for further processing. Depending on the signal quality a smooth template was constructed. Fig. 5 depicts the results at different stages of the template generation procedure.

Template delineation: Template delineation yields the template's fiducial points, i.e. points that carry diagnostic information. The onset of the Q wave and the end of the T-wave are defined in the template and tracked afterwards. Fiducial points are located by comparing the derivate of the signal to predefined thresholds [33]. The search for threshold crossings and flat sections is carried out in predefined time windows. Those windows are gained by using the mean RR_i of the beats which established the template and Bazett's normalized QT estimate

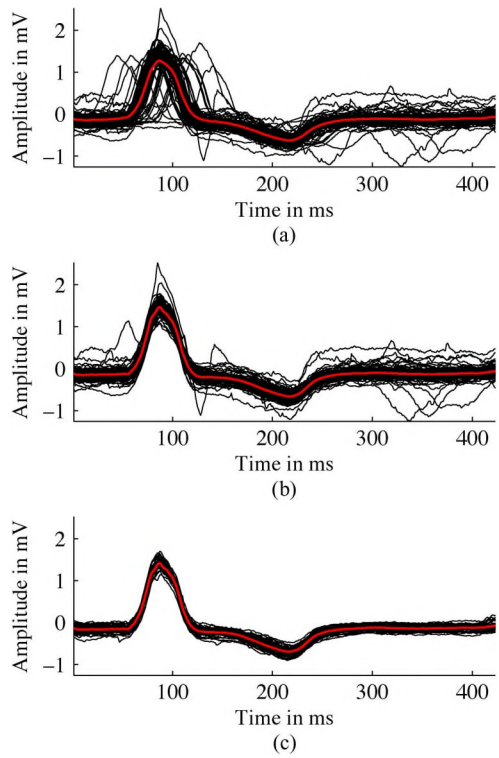

Fig. 5. Superimposed QT windows of single beats (black) and the resulting mean QT window (red) at different stages of the template construction. (a) Before alignment; (b) after alignment by TDE; (c) after removal of inappropriate beats.

[34]. The software program allows for manual editing of fiducial points, similar to other programs [24].

C. Application of Warping

Grid preparation: Template segmentation refers to all operations that are related to the warping grid. In general, 2DSW supports an arbitrary number and arrangement of horizontal and vertical segments. For the current application we divided the template in vertical direction homogeneously into 3 segments.

In horizontal direction we performed an inhomogeneous segmentation into 6 segments. The segments were fixed automatically on the basis of piecewise linear approximation (PLA) as proposed by Keogh *et al.* [10]. PLA approximates a signal with straight lines by minimizing the residual. Consequently, line breaks occur where the slope of the signal changes abruptly. We established the segment borders halfway in-between the breaks of approximation lines (see Fig. 6) so that each segment contains some variation in the signal. The vertical segmentation was carried out uniformly, i.e. the overall signal range was divided into three segments. The warping range for each point P_i in each direction was 20% of the distance to its neighbouring warping point in that direction (The range was set empirically. In principle the algorithm supports arbitrary deviations). The temporal resolution for shifting warping points was 1 sample. The amplitude resolution was set to 1 μV.

2DSW of each segment: 2DSW for each segments incorporates the procedure described in algorithm 1 applied to each beat. The current beat is regarded as reference to which the template adapts.

QT interval calculation: Based on the location of the fiducial points in the optimally warped template the QT interval of the current beat is extracted.

D. Post-Processing

Beat rejection: Beat rejection is directed at removing unusable heart beats. The applied post-processing scheme assumes that 2DSW is generally able to match the template closely to the reference waveform. If only a poor matching can be achieved the beat under consideration is likely to be corrupted by noise, incorrect QRS annotations or ectopic and excluded from further analysis. A beat is excluded if the normalized Manhattan distance (see (20)) exceeds 100 $\mu\mathrm{V}/\mathrm{Sample}$. We parameterized the exclusion criterion, i.e. determined the threshold for exclusion, empirically so that exclusion rates similar to those reported by Hasan *et al.* [27] were achieved for the real data (see below).

QTV quantification: After excluding unusable beats QTV is assessed by calculating the standard deviation QT_{sd} of the remaining QT intervals. Other commonly used QTV metrics such as the QT variability index can be easily implemented.

E. Performance Evaluation Using Simulated and Real ECG

To evaluate the performance of our method with respect to accurateness against typical factors known to affect QT measurement we used simulated data previously described by Porta *et al.* [35]. Briefly, a simulated ECG is composed of a single heart beat, which was repeated 500 times (the single beat was extracted from lead II of an ECG recorded at 1000 Hz with 12 bit amplitude resolution). The degree of difficulty to determine the QT interval was varied by lowering the T-wave amplitude A_T of the template beat in steps of 1/10 A_T to 1/10 A_T. Thus, 10 recordings of decreasing T-wave amplitude were obtained. Additional distortions, namely white Gaussian noise, baseline wander or sinusoidal amplitude modulation of ECG, were introduced resulting in a total of 30 recordings overall. Given the constant QT interval, one would expect an algorithm to measure QTV equal to 0.

Baumert *et al.* [36] compared three algorithms, template stretch [24], template shift [37] and a conventional (derivative) approach [35], and showed that using these data the template based algorithms outperform the other method in most cases. However, the authors emphasize certain limitations of the comparison, arising e.g. from differing beat rejection strategies. Moreover, as the artificial data do not necessarily comprise physiological variations of the QT interval one might not be able to deduce the best real world performance from this test. Nevertheless the data provide a good way to characterize a method's behavior in face of typical problems encountered in QT interval analysis. In our work, results obtained by using 2DSW are compared to the results of Baumert *et al.* [36].

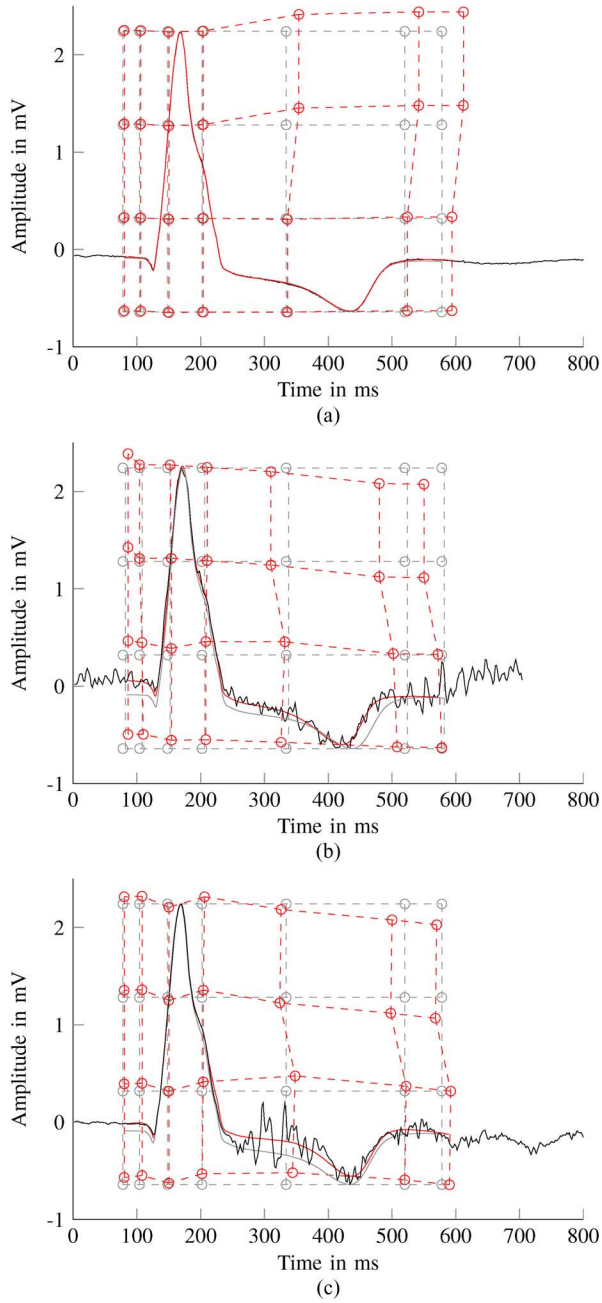

Fig. 6. Examples of templates before (gray) and after (bold red) adaptation to heart beats (black) by 2DSW. The warping grids are shown by gray (before) and red (after) dashed lines. 2DSW yielded normalized Euclidean distances of 0.4 (a), 3.7 (b) and 5.7 (c), respectively. (a) Example with low noise. (b) Example with noise. (c) Example with spikes.

To assess the sensitivity of the proposed method to capture pathophysiological QT variability, we used real recordings from the PTB Diagnostic ECG Database [38], which is freely available on Physionet [39]. These data have previously been applied by Hasan *et al.* [27] to investigate if

1) post myocardial infarction (MI) patients can be distinguished from healthy controls by using QTV.
2) there are differences in QTV and T-wave amplitudes as derived from different leads.

In detail, 79 MI patients (22 female, mean age 63 $\pm$ 12 years; 57 male, mean age 57 $\pm$ 10 years) and 69 healthy subjects (17 female, 42 $\pm$ 18 years; 52 male, 40 $\pm$ 13 years) were considered. Standard resting 12-lead ECGs that were recorded between one and two weeks after the infarction date were considered for this study. The duration of recording was on average 2 mins. The variability of the beat-to-beat RR intervals expressed as standard deviation is 44.89 ms in healthy subjects $\pm$ 20.80 ms and 35.91 ms $\pm$ 52.63 ms (mean $\pm$ std) in MI patients. To derive QT interval Hasan *et al.* used the template stretching method of Berger *et al.* [24] extended by a custom made pre-processing stage. Significant differences in QTV between different leads were reported which seem to be closely related to the varying T-wave amplitudes across leads. Further it was found that a differentiation of post-MI patients and healthy controls by using QTV is possible where lead II distinguished the groups most effectively.

The present work seeks to compare selected results published in [27] to the ones obtained by using our processing scheme, including 2DSW. We compared QTV obtained from lead II in MI patients and healthy controls because significant differences would be expected. Differences between MI patients and healthy controls are assessed by using the student t-test.

In addition, we used the QT database (QTDB), which is freely available on Physionet [40], to compare measured beat-to-beat QT interval changes to manual and automated annotations obtained with other methods. The database was designed for the evaluation of algorithms for the measurement of QT and other time intervals in ECG. The QTDB consists of 105 fifteen-minute excerpts of two-channel ECG Holter recordings. The recordings include a broad variety of QRS and ST-T morphologies. Each recording contains reference annotations for at least 30 heart cycles. Templates were constructed as described in Section III-B. To minimize the influence of manually set annotations the QT interval in the template was automatically derived from three reference annotations of the annotated beats that resemble the template most closely. Strategies for the measurement and evaluation of time intervals using the QTDB differ between methods and researchers. Algorithmic measurements most often make use of a single lead only, whereas the reference annotation of the QTDB is based on two leads. One commonly used procedure involves delineation in a single channel and comparing the algorithmic results to the reference (*single lead evaluation*). Another strategy involves delineating in the two leads independently and incorporating the reference annotation to select the algorithmic annotation that best matches the reference annotation for each beat (*supervised two lead evaluation*) [41].

IV. Results

Fig. 6 gives examples of templates that were adapted to single beats by using 2DSW.

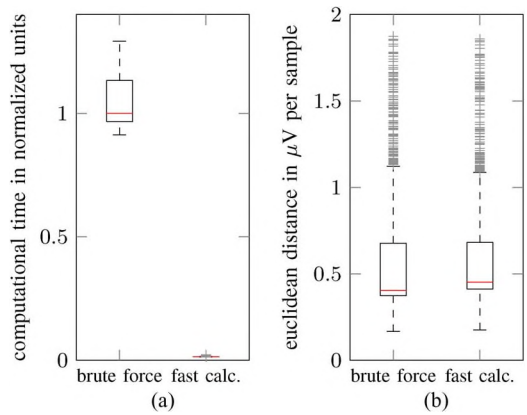

Fig. 7. Comparison of brute force and fast calculation methods for finding the optimum of the adaptation matrix. Computational times are normalized by the median computational time of the brute force method. We used a standard PC (6 CPU cores, 8 GB RAM). The computing time per beat was 14.9 s (brute force) and 0.2 s (fast calculation). (a) Computational time. (b) Euclidean distance.

Fig. 7 compares the computational times that result from using the brute force method to those spent by using the fast calculation. Additionally, the degree of matching between the adapted waveforms and its reference in terms of a normalized Euclidean distance is shown. The fast calculation significantly increased the computational efficiency ($p < 0.001$, using student t-test applied to computational times) while providing comparable results with respect to template adaptation. The algorithm reduces the median computational time by factor 71. Fig. 7 also illustrates the effectiveness of the proposed heuristic to find the optimum of the adaptation matrix. The median degree of adaptation in terms of normalized Euclidean distance stays below 0.5, which corresponds to close matching (see Fig. 6 for an illustration of different degrees of matching).

Fig. 8 shows the results that have been obtained by applying 2DSW to simulated data. Our results are compared to those presented in [36]. Our algorithm outperforms the other algorithms in the presence of white Gaussian noise and ECG amplitude modulation, while it performs second best during simulated baseline wander. Taken together, i.e. averaged over noises types and strength, 2DSW improved the results by 30% (i.e. measured QTV is 30% lower than the second best method, paired one-tailed Student's t-test: $p < 0.05$).

Fig. 9 shows the results that have been obtained by applying 2DSW to real data. Post-processing excluded 0.2% of the beats in normal subjects and 1.1% of the beats in the MI group. Our results are compared to the ones obtained by Hasan *et al.* [27] for the same task. A two-way ANOVA (factors: method and population) revealed a significant difference ($p < 0.001$) for the factor population. Both methods, 2DSW and template stretch, show highly significant difference between MI and healthy controls (pairwise testing using student-t-test). Using a F-test we found no significant difference between the methods regarding inter-subject variability (healthy $p = 0.0837$, MI $p = 0.4765$).

Table I shows the results of QRS-onset and T-end calculation by 2DSW using QTDB in comparison to other methods. Mean errors and standard deviations of 2DSW were computed by averaging the intrarecording mean errors and standard deviations. Because 2DSW is directed at capturing beat-to-beat

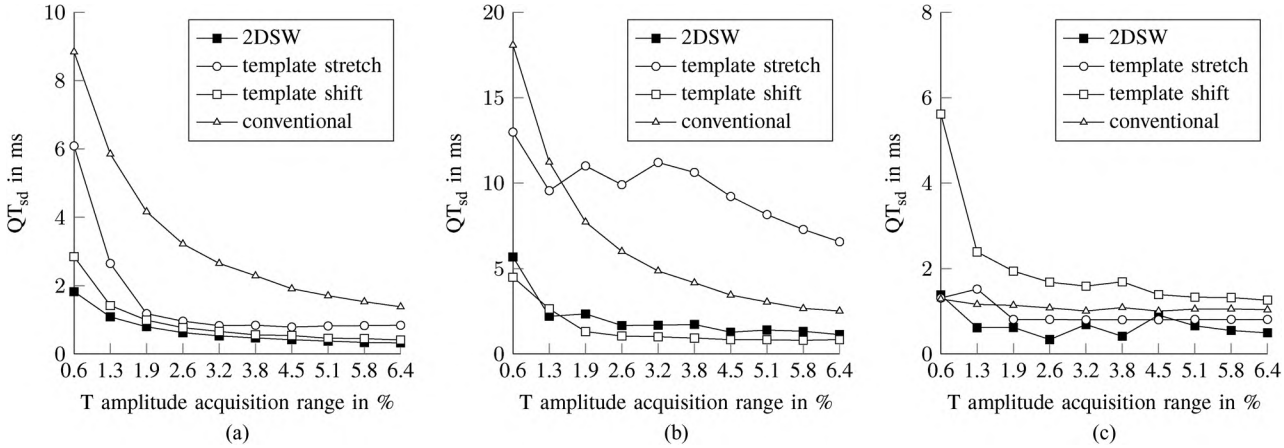

Fig. 8. Results obtained with the 2DSW algorithm (fast calculation) in comparison to previously published algorithms using simulated data with zero QTV [36]. White Gaussian noise, baseline wander or sinusoidal amplitude modulation were introduced resulting in a total of 30 recordings. Lower QTV values refer to a more accurate measurement. (a) White Gaussian noise. (b) Baseline wander. (c) Amplitude Modulation.

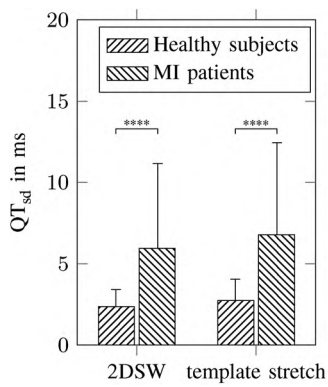

Fig. 9. QTV results obtained with the 2DSW algorithm (fast calculation) in comparison to the template stretching method for MI patients and healthy controls.

TABLE I
QTDB Results Obtained With 2DSW and Other Methods. Mean Errors and Standard Deviations of 2DSW Were Computed by Averaging the Intrarecording Mean Errors and Standard Deviations

Method (used lead)	Q-onset Se*	Q-onset mean	Q-onset std	T-end Se*	T-end mean	T-end std
single lead evaluation (all results in ms)						
Zifan [25] (2)	74.8	-5.22	3.60	63.4	6.72	33.5
Vullings [42] (1)	81.5	-0.8	10.6	79.4	9.4	49.0
Dubois [43] (1)	n.a.	n.a.	n.a.	82.1	45.0	38.6
Dubois [43] (2)	n.a.	n.a.	n.a.	81.6	42.8	40.3
Rincon [44] (1)	99.6	5.4	8.4	99.3	-5.3	22.7
Rincon [44] (2)	99.7	8.6	12.6	99.2	-4.6	27.2
2DSW (1)	88.3	-4.1	7.1	90.3	-5.6	15.1
2DSW (2)	88.6	-6.0	7.9	90.7	-6.8	16.5
supervised two lead evaluation (all results in ms)						
Martinez [41]	100	4.6	7.7	99.8	-1.6	18.1
Laguna [41]**	99.9	-3.6	8.6	99.0	13.5	27.0
Dubois [43]	n.a.	n.a.	n.a.	93.6	34.8	30.3
Rincon [44]	100	3.4	7.0	100	-2.4	16.9
2DSW	92.6	-3.0	6.1	94.7	-3.7	12.8

*Se in % is the sensitivity, i.e. the percentage of evaluated beats. For 2DSW all QRS reference annotations were considered. A beat was rejected, if 2DSW failed to adapt the template closely to that beat thus degrading SE.
**Numerical results were taken from Martinez *et al.* [41] who evaluated the method of Laguna *et al.* [33]], using the same evaluation scheme that we used.

changes, the algorithmic capacity is assessed best by the standard deviation, whereas the mean deviation is of minor interest. Our results show lower standard deviations compared to most other algorithms while the number of evaluated beats compares to the average usage rate.

Fig. 10 shows Bland-Altmann plots of the measured QT intervals and manually annotated QT intervals of QTDB. No dependence of the differences between referenced and the calculated QT interval to the mean QT interval is recognizable.

V. Discussion

In this contribution we presented the theoretical fundamentals and application of a technique for 2d adaptation of two 1d patterns. To the best of our knowledge this is the first time that 2d deformation of 1d signals was addressed in the way we presented here. 2DSW constitutes a powerful technique to quantify the similarity between patterns. By employing two-dimensional piecewise stretching 2DSW is able to take into account inhomogeneous variations in shape. In comparison to DTW approaches that have been used before in signal processing, 2DSW does not require amplitude normalization that is essential to other methods [45]. By avoiding a global normalization but introducing segmented adaptation 2DSW allows for more flexibility. Simulation studies showed high robustness of our approach in presence of typical ECG artefacts. Comparison of short-term ECG recorded in normal subjects versus patients with myocardial infarction (MI) showed significantly increased QTV in patients.

A. QT Evaluation

Our method proves to be very effective for QT interval extraction. Using simulated data 2DSW yields in almost all situations accurate results. Using real data, the sensitivity, i.e. the capability of the method to find differences between MI patients and healthy controls, is comparable. A slight decrease in QTV was observed in healthy subjects and MI patients when using 2DSW compared to Hasan *et al.* [27] while between-group differences were similar; the latter demonstrating equivalent sensitivity to

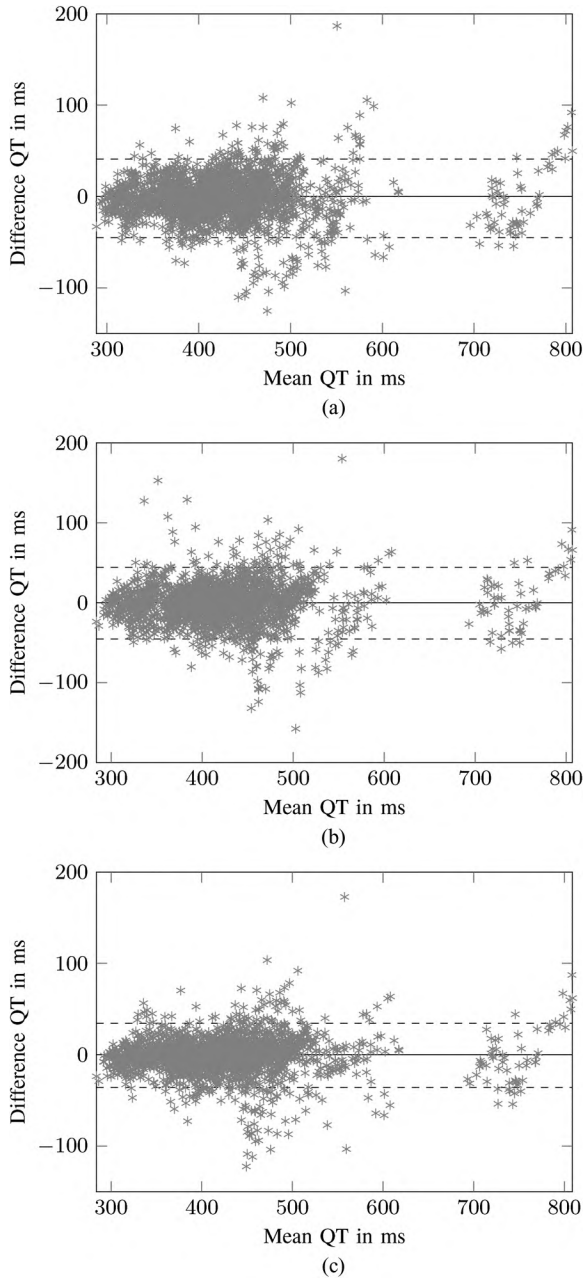

Fig. 10. Bland-Altman plots for reference QT intervals and QT intervals calculated by 2DSW. Mean differences are shown by black lines, upper and lower limits are shown by black dashed lines. (a) Bland-Altman plot of lead one. Mean difference: −2.2 ms, upper limit 40.9 ms, lower limit −45.2 ms, outliers 5.0%. (b) Bland-Altman plot of lead two. Mean difference: −0.4 ms, upper limit 44.5 ms, lower limit −45.3 ms, outliers 4.7%. (c) Bland-Altman plot of supervised two lead evaluation. Mean difference: −0.8 ms, upper limit 34.4 ms, lower limit −36.0 ms, outliers 5.3%.

temporal repolarization heterogeneity. The F-test shows no significant differences between the methods, i.e. similar inter-subject variabilities, which points to a likewise behavior of 2DSW. Taken together, similar sensitivity but increased robustness, the proposed method based on 2DSW is a very promising approach to extract the QT interval. However, our results need to be validated with different data sets. The results obtained by 2DSW using the QTDB are competitive with the most accurate results that have been published. However, our algorithm uses a-priori information by incorporating three reference cycles to construct the waveform boundaries of our template. Aiming at beat-to-beat QT variability extraction this step does not imply a fundamental restriction, but it shows 2DSW superiority compared to delineation methods that aim at a fully automated measurement. When evaluating the results in terms of absolute values one should also consider the limitations of the reference annotations. Although those annotations are regarded as gold standard, the comparison of reference annotations by two human annotators for selected records of the QTDB revealed deviations (mean $\pm$ std) of 5.3 ms $\pm$ 11.1 ms and 2.1 ms $\pm$ 22.4 ms for QRS-onset and T-end, respectively. Bland-Altman plots show no systematic under- or overestimation of short and long QT intervals.

When comparing the performance between software implementations of different algorithms one should bear in mind that quantitative assessment of QTV not only depends 2DSW, but may also be affected by other algorithmic steps such as beat rejection. Beat rejection aims at the exclusion of beats for which an accurate QT interval cannot be obtained. An insufficient template adjustment by 2DSW is indicative of such cases. The observation of higher exclusion rates in MI patients compared to normal subjects, which is probably caused by a higher number of abnormal beats, suggests effective beat rejection criteria. However, the lack of an empirical value for the degree of adjustment in face of technical and/or pathophysiological impact factors renders the definition of threshold values for beat rejection difficult. For comparability, we parameterized the exclusion criterion so that exclusion rates similar to those reported by Hasan *et al.* [27] were achieved. The same parameter setting has been applied to the simulated data, where no single beat had to be discarded because of the beat rejection procedure. Baumert *et al.* showed the template stretch algorithm to produce high exclusion rates, particularly for baseline drift and amplitude modulation [36]. 2DSW appears to cope particularly well with those conditions. However, a thorough examination of beat rejection criteria should be carried out in the future.

Besides the strategy for beat rejection, the template construction is assumed to affect the results. We decided to use a conventional approach instead of incorporating 2DSW in the template generation process. Caiani *et al.* successfully included DTW in the template generation [45]. However, even though including DTW in the template generation is, in principle, more adequate to follow the stretching and shrinking of the cardiac cycle due to the variability of heart period, the performance of the adopted conventional template construction procedure was remarkable. Future studies should focus on introducing 2DSW in the template construction and testing whether this introduction further improves the performance of the proposed method.

B. Comparison of the Proposed 2DSW With Other Algorithms

2DSW utilizes features that are typical for DTW and COW. In analogy to DTW, a distance measure is used that incorporates information on the signal's amplitude. The partitioning into segments, on the other hand, strongly relates to COW. To overcome the lack of robustness of DTW concerning signal artifacts and local differences in amplitude values [10], 2DSW introduces piecewise amplitude normalization. By segmenting the signal, a higher robustness can be achieved by the preserving signal characteristics. A conceptual difference exists regarding the boundary condition. Many variants of DTW and

COW project the first and last data points of the pattern to be compared to each other. This restriction is avoided in our implementation. Moreover, the implementation of DTW and COW usually find the global optimum in terms of the cost function to be optimized. Thus, the applied strategy of dynamic programming requires the evaluation of many possible combinations of shifts. 2DSW expands the search space vastly. A procedure similar to those used in 1d warping is computationally not feasible in case of 2DSW. We thus introduced a heuristic procedure to solve the optimization problem imposed by 2DSW. Multiscale search procedures within the heuristic may further speed up computations.

As 2d warping approaches have been previously described in the literature it is important to distinguish 2DSW from previously proposed methods, which have been used for image processing. Both, DTW and COW have been adapted to 2d warping of 2d images [46]–[48]. In the context of image processing warping does not account for temporal shifts, but for spatial ones. They are performed on pixels and pixel intensities, while our approach focuses on signals.

VI. Conclusions

The two-dimensional warping approach introduced in this paper is able to detect subtle changes in noisy quasi-periodic biomedical signals. We illustrated its implementation for ECG processing and demonstrated its performance by measuring beat-to-beat QT interval variability in simulations and clinical data. 2DSW might also be beneficial to solve problems where 1d warping techniques have been used in the past [7], [8]. More generally, 2DSW might be useful in situations where coherent averaging of signals is used to increase the SNR or construct templates [32], [49].

References

[1] T. K. Vintsyuk, "Speech discrimination by dynamic programming," *Cybernetics*, vol. 4, no. 1, pp. 52–57, 1968.

[2] V. Velichko and N. Zagoruyko, "Automatic recognition of 200 words," *Int. J. Man. Mach. Stud.*, vol. 2, no. 3, pp. 223–234, Jul. 1970.

[3] H. Sakoe and S. Chiba, "Dynamic programming algorithm optimization for spoken word recognition," *IEEE Trans. Acoust., Speech, Signal Process.*, vol. 26, no. 1, pp. 43–49, 1978.

[4] M. Faundez-Zanuy, "On-line signature recognition based on VQ-DTW," *Pattern Recogn.*, vol. 40, no. 3, pp. 981–992, Mar. 2007.

[5] F. Hermans and E. Tsiporkova, "Merging microarray cell synchronization experiments through curve alignment," *Bioinformat.*, vol. 23, no. 2, pp. e64–e70, Jan. 2007.

[6] P. M. P. Jayadevan R and S. R. Kolhe, "Dynamic time warping based static hand printed signature verification," *J. Pattern Recogn. Res.*, vol. 1, pp. 52–65, 2009.

[7] Q. Li and G. D. Clifford, "Dynamic time warping and machine learning for signal quality assessment of pulsatile signals," *Physiol. Meas.*, vol. 33, no. 9, p. 1491, Sep. 2012.

[8] H. J. L. M. Vullings, M. H. G. Verhaegen, and H. B. Verbruggen, "ECG segmentation using time-warping," in *Advances in Intelligent Data Analysis Reasoning about Data*, ser. Lecture Notes in Comput. Sci., X. Liu, P. Cohen, and M. Berthold, Eds. Berlin, Germany: Springer, Jan. 1997, pp. 275–285, no. 1280.

[9] E. Keogh and M. Pazzani, "Scaling up dynamic time warping to massive datasets," in *Principles of Data Mining and Knowledge Discovery*, J. Żytkow and J. Rauch, Eds. Berlin, Germany: Springer, 1999, pp. 1–11.

[10] E. J. Keogh and M. J. Pazzani, "Derivative dynamic time warping," presented at the 1st SIAM Int. Conf. Data Mining, Chicago, IL, USA, 2001.

[11] S. Salvador and P. Chan, "Toward accurate dynamic time warping in linear time and space," *Intell. Data Anal.*, vol. 11, no. 5, pp. 561–580, Oct. 2007.

[12] A. Arzt, G. Widmer, and S. Dixon, "Automatic page turning for musicians via real-time machine listening," in *Proc. Conf. ECAI 2008: 18th European Conference on Artificial Intelligence*. Amsterdam, The Netherlands: IOS Press, 2008, pp. 241–245.

[13] N.-P. V. Nielsen, J. M. Carstensen, and J. Smedsgaard, "Aligning of single and multiple wavelength chromatographic profiles for chemometric data analysis using correlation optimised warping," *J. Chromatogr. A*, vol. 805, no. 1–2, pp. 17–35, May 1998.

[14] G. Tomasi, F. van den Berg, and C. Andersson, "Correlation optimized warping and dynamic time warping as preprocessing methods for chromatographic data," *J. Chemom.*, vol. 18, no. 5, pp. 231–241, 2004.

[15] A. M. van Nederkassel, M. Daszykowski, P. H. C. Eilers, and Y. V. Heyden, "A comparison of three algorithms for chromatograms alignment," *J. Chromatogr. A*, vol. 1118, no. 2, pp. 199–210, Jun. 2006.

[16] V. Pravdova, B. Walczak, and D. Massart, "A comparison of two algorithms for warping of analytical signals," *Anal. Chim. Acta*, vol. 456, no. 1, pp. 77–92, Apr. 2002.

[17] G. Piccirillo, D. Magrì, S. Matera, M. Magnanti, A. Torrini, E. Pasquazzi, E. Schifano, S. Velitti, V. Marigliano, R. Quaglione, and F. Barillà, "QT variability strongly predicts sudden cardiac death in asymptomatic subjects with mild or moderate left ventricular systolic dysfunction: A prospective study," *Eur. Heart J.*, vol. 28, no. 11, pp. 1344–1350, Jun. 2007.

[18] S. Nayyar, K. C. Roberts-Thomson, M. A. Hasan, T. Sullivan, J. Harrington, P. Sanders, and M. Baumert, "Autonomic modulation of repolarization instability in patients with heart failure prone to ventricular tachycardia," *Amer. J. Physiol. Heart Circ. Physiol.*, vol. 305, no. 8, pp. H1181–H1188, Oct. 2013.

[19] J. W. Sacre, B. Franjic, J. S. Coombes, T. H. Marwick, and M. Baumert, "QT interval variability in type 2 diabetic patients with cardiac sympathetic dysinnervation assessed by 123i-metaiodobenzylguanidine scintigraphy," *J. Cardiovasc. Electrophysiol.*, vol. 24, no. 3, pp. 305–313, Mar. 2013.

[20] G. Valenza, L. Citi, E. Scilingo, and R. Barbieri, "Point-process nonlinear models with Laguerre and Volterra expansions: Instantaneous assessment of heartbeat dynamics," *IEEE Trans. Signal Process.*, vol. 61, no. 11, pp. 2914–2926, Jun. 2013.

[21] A. Mincholé, E. Pueyo, J. Rodríguez, E. Zacur, M. Doblaré, and P. Laguna, "Quantification of restitution dispersion from the dynamic changes of the t-wave peak to end, measured at the surface ECG," *IEEE Trans. Biomed. Eng.*, vol. 58, no. 5, pp. 1172–1182, May 2011.

[22] R. Sassi and L. Mainardi, "An estimate of the dispersion of repolarization times based on a biophysical model of the ECG," *IEEE Trans. Biomed. Eng.*, vol. 58, no. 12, pp. 3396–3405, Dec. 2011.

[23] R. D. Berger, "Methodology for automated QT variability measurement," Oct. 1996 [Online]. Available: http://www.google.com/patents/US5560368

[24] R. D. Berger, E. K. Kasper, K. L. Baughman, E. Marban, H. Calkins, and G. F. Tomaselli, "Beat-to-beat QT interval variability: Novel evidence for repolarization lability in ischemic and nonischemic dilated cardiomyopathy," *Circulation*, vol. 96, no. 5, pp. 1557–1565, Sep. 1997.

[25] A. Zifan, M. H. Moradi, S. Saberi, and F. Towhidkhah, "Automated segmentation of ECG signals using piecewise derivative dynamic time warping," *Int. J. Biolog. Life Sci.*, vol. 1, pp. 181–185, 2007.

[26] J.-L. Starck, J. Fadili, and F. Murtagh, "The undecimated wavelet decomposition and its reconstruction," *IEEE Trans. Image Process.*, vol. 16, no. 2, pp. 297–309, Feb. 2007.

[27] M. A. Hasan, D. Abbott, and M. Baumert, "Beat-to-beat QT interval variability and t-wave amplitude in patients with myocardial infarction," *Physiol. Meas.*, vol. 34, no. 9, p. 1075, Sep. 2013.

[28] V. Afonso, W. J. Tompkins, T. Nguyen, and S. Luo, "ECG beat detection using filter banks," *IEEE Trans. Biomed. Eng.*, vol. 46, no. 2, pp. 192–202, Feb. 1999.

[29] C. Vidaurre, T. H. Sander, and A. Schlögl, "BioSig: The free and open source software library for biomedical signal processing," *Computat. Intell. Neurosci.*, vol. 2011, p. e935364, Mar. 2011.

[30] A. Cabasson and O. Meste, "Time delay estimation: A new insight into the Woody's method," *IEEE Signal Process. Lett.*, vol. 15, pp. 573–576, 2008.

[31] P. Laguna, G. B. Moody, J. García, A. L. Goldberger, and R. G. Mark, "Analysis of the ST-t complex of the electrocardiogram using the karhunen—Loeve transform: Adaptive monitoring and alternans detection," *Med. Biolog. Eng. Comput.*, vol. 37, no. 2, pp. 175–189, Mar. 1999.

[32] O. Rompelman and H. H. Ros, "Coherent averaging technique: A tutorial review. Part 1: Noise reduction and the equivalent filter," *J. Biomed. Eng.*, vol. 8, no. 1, pp. 24–29, Jan. 1986.

[33] P. Laguna, R. Jané, and P. Caminal, "Automatic detection of wave boundaries in multilead ECG signals: Validation with the CSE database," *Comput. Biomed. Res.*, vol. 27, no. 1, pp. 45–60, Feb. 1994.

[34] H. C. Bazett, "An analysis of the time relation of electrocardiograms," *Heart*, vol. 7, pp. 353–370, 1920.

[35] A. Porta, G. Baselli, F. Lambardi, S. Cerutti, R. Antolini, M. D. Greco, F. Ravelli, and D. G. Nollo, "Performance assessment of standard algorithms for dynamic r-t interval measurement: Comparison between r-tapex and r-tend approach," *Med. Biol. Eng. Comput.*, vol. 36, no. 1, pp. 35–42, Jan. 1998.

[36] M. Baumert, V. Starc, and A. Porta, "Conventional QT variability measurement vs. template matching techniques: Comparison of performance using simulated and real ECG," *PLoS ONE*, vol. 7, no. 7, p. e41920, Jul. 2012.

[37] V. Starc and T. T. Schlegel, "Real-time multichannel system for beatto-beat QT interval variability," *J. Electrocardiol.*, vol. 39, no. 4, pp. 358–367, Oct. 2006.

[38] R. Bousseljot, D. Kreiseler, and A. Schnabel, "Nutzung der EKG-signaldatenbank CARDIODAT der PTB über das Internet," *Biomedizinische Technik/Biomed. Eng.*, pp. 317–318, Jul. 1995.

[39] A. L. Goldberger, L. A. Amaral, L. Glass, J. M. Hausdorff, P. C. Ivanov, R. G. Mark, J. E. Mietus, G. B. Moody, C. K. Peng, and H. E. Stanley, "PhysioBank, PhysioToolkit, PhysioNet: Components of a new research resource for complex physiologic signals," *Circulation*, vol. 101, no. 23, pp. E215–E220, Jun. 2000.

[40] P. Laguna, R. Mark, A. Goldberg, and G. Moody, "A database for evaluation of algorithms for measurement of QT and other waveform intervals in the ECG," in *Proc. Comput. Cardiol.*, 1997, pp. 673–676.

[41] J. P. Martinez, R. Almeida, S. Olmos, A. P. Rocha, and P. Laguna, "A wavelet-based ECG delineator: Evaluation on standard databases," *IEEE Trans. Biomed. Eng.*, vol. 51, no. 4, pp. 570–581, Apr. 2004.

[42] H. J. L. M. Vullings, M. H. G. Verhaegen, and H. Verbruggen, "Automated ECG segmentation with dynamic time warping," in *Proc. 20th Ann. IEEE Int. Conf. Eng. Med. Biol. Soc.*, 1998, vol. 1, pp. 163–166.

[43] R. Dubois, P. Maison-Blanche, B. Quenet, and G. Dreyfus, "Automatic ECG wave extraction in long-term recordings using Gaussian mesa function models and nonlinear probability estimators," *Comput. Methods Programs Biomed.*, vol. 88, no. 3, pp. 217–233, Dec. 2007.

[44] F. Rincón, J. Recas, N. Khaled, and D. Atienza, "Development and evaluation of multilead wavelet-based ECG delineation algorithms for embedded wireless sensor nodes," *IEEE Trans. Inf. Technol. Biomed.*, vol. 15, no. 6, pp. 854–863, Nov. 2011.

[45] D. E. G. Caiani, A. Porta, G. Baselli, M. Turiel, S. Muzzupappa, M. Pagani, A. Malliani, and S. Cerutti, "Analysis of cardiac leftventricular volume based on time warping averaging," *Med. Biol. Eng. Comput.*, vol. 40, no. 2, pp. 225–233, Mar. 2002.

[46] K. C. Chu S and S. Narayanan, "Efficient rotation invariant retrieval of shapes with applications in medical databases," in *Proc. IEEE 19th Symp. Comput.-Based Med. Syst. (CBMS)*, 2006, pp. 673–678.

[47] S. Wang, J. Yao, J. Liu, N. Petrick, R. L. V. Uitert, S. Periaswamy, and R. M. Summers, "Registration of prone and supine CT colonography scans using correlation optimized warping and canonical correlation analysis," *Med. Phys.*, vol. 36, no. 12, pp. 5595–5603, Dec. 2009.

[48] D. Zhang, X. Huang, F. E. Regnier, and M. Zhang, "Two-dimensional correlation optimized warping algorithm for aligning GC × GC-MS data," *Anal. Chem.*, vol. 80, no. 8, pp. 2664–2671, Apr. 2008.

[49] R. Sameni, M.-B. Shamsollahi, C. Jutten, and G. Clifford, "A nonlinear Bayesian filtering framework for ECG denoising," *IEEE Trans. Biomed. Eng.*, vol. 54, no. 12, pp. 2172–2185, Dec. 2007.

Martin Schmidt received the M.Sc. degree in electrical engineering and computer science from TU Dresden (TUD), Germany, in 2013. He is currently a Ph.D. student at the Institute of Biomedical Engineering of TUD.

His main research interest is biomedical signal processing, especially the analysis of the electrocardiograms.

Mathias Baumert (M'09–SM'13) received the Ph.D. degree in biomedical engineering from the Technical University Ilmenau, Germany, in 2005. Subsequently he was awarded the Australian Postdoctoral Fellowship and the Australian Research Fellowship from the Australian Research Council.

He is currently an Associate Professor at the School of Electrical & Electronic Engineering at the University of Adelaide, Australia. His research interests include processing of electrophysiological signals, computerized electrocardiography and electroencephalography, cardiac autonomic modulation, and sleep.

Alberto Porta (M'09) received the degree in Electronic Engineering at Polytechnic University of Milan, Milan, Italy in 1989 and the Ph.D. degree in Biomedical Engineering in the same University in 1998. Since 1999, he has been with the Faculty of Medicine, University of Milan, Milan, Italy where he has been Associate Professor since 2011.

His primary interests include time series analysis, biomedical signal processing, non linear dynamics, complexity analysis, system identification and modeling applied to cardiovascular control mechanisms.

Hagen Malberg received the Ph.D. degree in 1999.

From 1999 to 2010, he was head of Biosignal Processing Group (Karlsruhe Research Center and KITKarlsruhe Institute of Technology). Since 2010, he has been chair of Biomedical Engineering, TU Dresden. His research interests cover biosignal analysis, particularly related to the regulation of the cardiovascular system.

Sebastian Zaunseder received the Ph.D. degree in electrical engineering from TU Dresden (TUD), Germany, in 2011. Subsequently he joined the Institute of Biomedical Engineering of TUD where he is currently head of the group Medical Sensing and Signal Processing.

His research interests include contact-free measurement systems, processing of biomedical signals and images to acquire robust information on vital signs, investigations on the cardio-respiratory autonomic modulation and research related to sleep.